AGU PUBLICATIONS

Geochemistry, Geophysics, Geosystems

RESEARCH ARTICLE
10.1002/2016GC006715

Key Points:
- New MATLAB algorithm quantifies K, U, and Th contents in marine sediments from NGR spectra
- NGR-derived element contents have good accuracy and satisfactory precision
- The algorithm rapidly produces useful shipboard data (few minutes) at no extra cost

Supporting Information:
- Supporting Information S1
- Software S1
- Software S2
- Dataset S1–S3

Correspondence to:
D. De Vleeschouwer,
ddevleeschouwer@marum.de

Citation:
De Vleeschouwer, D., et al., (2017), Quantifying K, U, and Th contents of marine sediments using shipboard natural gamma radiation spectra measured on DV *JOIDES Resolution*, *Geochem. Geophys. Geosyst.*, *18*, 1053–1064, doi:10.1002/2016GC006715.

Received 9 NOV 2016
Accepted 16 FEB 2017
Accepted article online 20 FEB 2017
Published online 21 MAR 2017
Corrected 21 MAR 2017

This article was corrected on 31 MAR 2017. See the end of the full text for details.

Quantifying K, U, and Th contents of marine sediments using shipboard natural gamma radiation spectra measured on DV *JOIDES Resolution*

David De Vleeschouwer[1], Ann G. Dunlea[2,3], Gerald Auer[4], Chloe H. Anderson[2], Hans Brumsack[5], Aaron de Loach[6], Michael Gurnis[7], Youngsook Huh[8], Takeshige Ishiwa[9], Kwangchul Jang[8], Michelle A. Kominz[10], Christian März[11], Bernhard Schnetger[5], Richard W. Murray[2], Heiko Pälike[1], and Expedition 356 Shipboard Scientists[12]

[1]MARUM - Center for Marine Environmental Science, University of Bremen, Bremen, Germany, [2]Department of Earth and Environment, Boston University, Boston, Massachusetts, USA, [3]Department of Geology and Geophysics, Woods Hole Oceanographic Institution, Woods Hole, Massachusetts, USA, [4]Institute of Earth Sciences, University of Graz, NAWI Graz Geocenter, Graz, Austria, [5]Institute for Chemistry and Biology of the Marine Environment (ICBM), University of Oldenburg, Oldenburg, Germany, [6]International Ocean Discovery Program, Texas A&M University, College Station, Texas, USA, [7]Division of Geological and Planetary Sciences, California Institute of Technology, Pasadena, California, USA, [8]School of Earth and Environmental Sciences, Seoul National University, Seoul, South Korea, [9]Atmosphere and Ocean Research Institute, The University of Tokyo, Chiba, Japan, [10]Department of Geosciences, Western Michigan University, Kalamazoo, Michigan, USA, [11]School of Earth and Environment, University of Leeds, Leeds, UK, [12]http://iodp.tamu.edu/scienceops/precruise/indonesianthruflow/participants.html

Abstract During International Ocean Discovery Program (IODP) expeditions, shipboard-generated data provide the first insights into the cored sequences. The natural gamma radiation (NGR) of the recovered material, for example, is routinely measured on the ocean drilling research vessel DV *JOIDES Resolution*. At present, only total NGR counts are readily available as shipboard data, although full NGR spectra (counts as a function of gamma-ray energy level) are produced and archived. These spectra contain unexploited information, as one can estimate the sedimentary contents of potassium (K), thorium (Th), and uranium (U) from the characteristic gamma-ray energies of isotopes in the ^{40}K, ^{232}Th, and ^{238}U radioactive decay series. *Dunlea et al.* (2013) quantified K, Th, and U contents in sediment from the South Pacific Gyre by integrating counts over specific energy levels of the NGR spectrum. However, the algorithm used in their study is unavailable to the wider scientific community due to commercial proprietary reasons. Here, we present a new MATLAB algorithm for the quantification of NGR spectra that is transparent and accessible to future NGR users. We demonstrate the algorithm's performance by comparing its results to shore-based inductively coupled plasma-mass spectrometry (ICP-MS), inductively coupled plasma-emission spectrometry (ICP-ES), and quantitative wavelength-dispersive X-ray fluorescence (XRF) analyses. Samples for these comparisons come from eleven sites (U1341, U1343, U1366-U1369, U1414, U1428-U1430, and U1463) cored in two oceans during five expeditions. In short, our algorithm rapidly produces detailed high-quality information on sediment properties during IODP expeditions at no extra cost.

1. Introduction

Natural gamma radiation (NGR) is emitted when ^{40}K, ^{238}U, and ^{232}Th radioisotopes decay. The radiation emitted during radioactive disintegration occurs at discrete energy levels, which are characteristic for the different emitting isotopes. The NGR spectra obtained from cored marine sediments are composed of one emission peak of ^{40}K at 1460 keV, and numerous peaks for the ^{238}U and ^{232}Th series. The most distinctive peak in the ^{232}Th series occurs at 2620 keV (from ^{208}Tl). The U series is distinguished by the ^{214}Bi peak at 1760 keV [*Serra*, 1984, Figure 1].

The NGR system that is currently installed on the IODP drillship *JOIDES Resolution* has been operating since March 2009 (beginning with Expedition 317). The system measures the intensity of gamma radiation at 1024 different channels, or energy levels, between 0 and 3000 keV [*Vasiliev et al.*, 2011]. The NGR intensity measured at an energy level characteristic for K, U, or Th is proportional to the content of that element in

the sediment. Hence, the current NGR setup on *JOIDES Resolution* allows for an estimation of the K, U, and Th contents from the shipboard NGR energy spectra [*Gilmore*, 2011; *Dunlea et al*., 2013]. In this paper, we provide MATLAB codes that calculate the sedimentary K, U, and Th contents from the NGR spectra. We then compare the results of the algorithm to element contents measured by inductively coupled plasma mass and emission- spectrometry (ICP-MS and ICP-ES, respectively) and X-Ray fluorescence (XRF), as well as to downhole wireline logging NGR records, which are decomposed into K, U, and Th contents by Schlumberger Services (Figure 1).

Quantifying the element content of K, U, and Th provides high-resolution (10 cm) data for a wide variety of scientific pursuits. For example, the three element profiles can provide additional or more detailed tie points to improve stratigraphic correlation. The element contents can also provide insights into the mineralogy and geochemistry of the recovered material. In some marine sediment lithologies, Th and K are linked to the detrital clay fraction. However, high Th values can also indicate the presence of heavy minerals like zircon, allanite, and monazite or volcanic ashes [*Serra*, 1984]. Glauconitic minerals, on the other hand, have very low Th/K ratios [*Hassan and Hossin*, 1975; *Hassan et al*., 1976]. In sandstones, feldspars and micas are common constituents, which can be the hosts of K [*Myers and Bristow*, 1989; *Humphreys and Lott*, 1990; *Hurst*, 1990]. The U content in sediments contains detrital, authigenic, and diagenetic components. Sediments rich in organic material that are deposited under anoxic conditions may be enriched in authigenic U

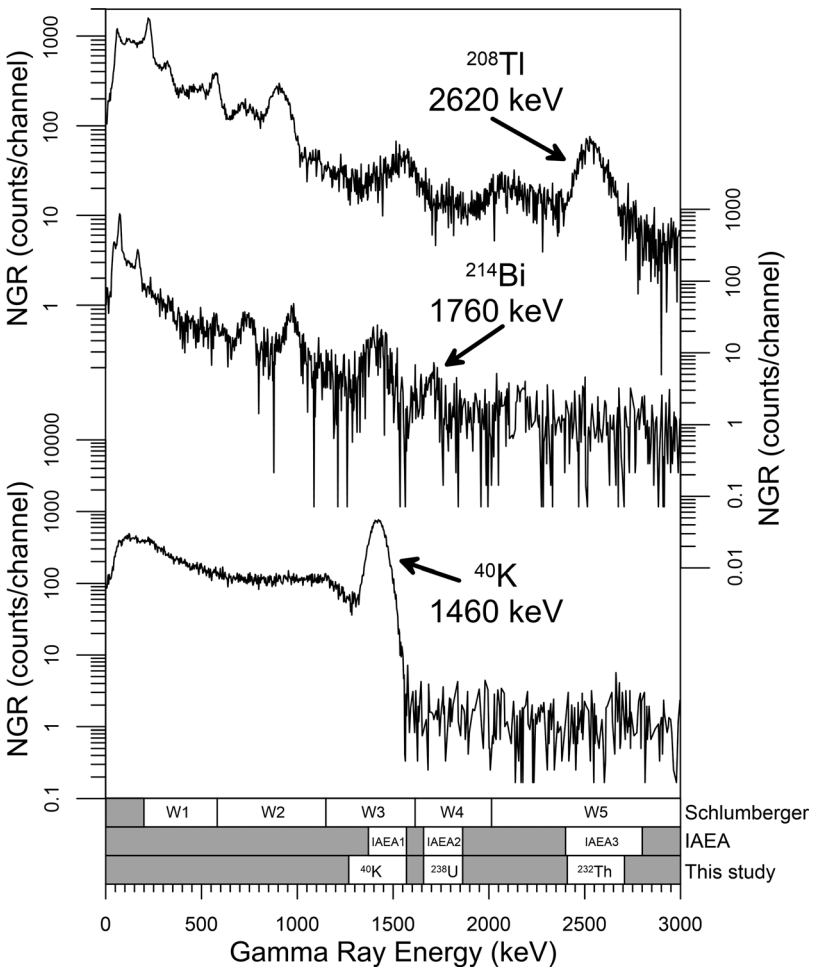

Figure 1. Natural gamma radiation spectrogram obtained during the measurement of K, Th, and U standards during 1500 s (for K and Th) and 1800 s (for U) after zero-background subtraction. The three spectrograms demonstrate the characteristic peaks for Th, U, and K, respectively. Our energy interval boundaries conform with intervals proposed by the IAEA [*International Atomic Energy Agency*, 1976], and with windows 3–5 that are used during wireline NGR spectrometry executed by Schlumberger Services on behalf of IODP's downhole measurement program [see also *Blum et al*., 1997]. In this study, we use three energy intervals to integrate counts, which are then compared between samples and standards to estimate the element content in the sample.

[*Brumsack*, 2006]. The relative enrichment of U over Th is often used to estimate redox conditions because Th is unaffected by redox conditions and remains in an insoluble state [*Adams and Weaver*, 1958; *Myers and Wignall*, 1987; *Doveton*, 1991; *Wignall and Twitchett*, 1996; *Bond and Zaton*, 2003; *De Vleeschouwer et al.*, 2013]. Anomalously high concentrations of U may also designate the presence of uranium-bearing phosphate nodules, perhaps associated with a hardground and a sedimentary unconformity. Microbiologists studying low levels of metabolic activity sustained by the radiolysis of pore waters within marine sediment [e.g., *D'Hondt et al.*, 2009] can use the contents of radioactive elements, quantified by NGR or other techniques, to estimate the amount of radiation inundating the porewater. In sediment deposited more recently than 1.5 Ma, these records may also be able to infer the presence of "excess" ^{230}Th and help estimate sedimentation rates.

2. Materials and Methods

2.1. Quantifying K, U, and Th Contents Using ICP-ES and ICP-MS

We evaluate the performance of the MATLAB algorithm by comparing its estimates of K, U, and Th contents to element data determined by inductively coupled plasma emission spectrometry (ICP-ES) and mass spectrometry (ICP-MS). ICP-ES and ICP-MS results from Site U1341 [Exp. 323; *Takahashi et al.*, 2011], Sites U1428–U1430 [Exp. 346; *Tada et al.*, 2015], and Site U1463 [Exp. 356; *Gallagher et al.*, 2014] were generated for this study (Figure 2). These data sets are complemented by previously published results from Sites U1366–U1369 [Exp. 329; *Dunlea et al.*, 2013] and Site U1414 [Exp. 344; *Yan and Shi*, 2016; Figure 2]. Samples from Expeditions 323, 346, and 356 were measured at the Korean Basic Science Institute (KBSI; Republic of Korea), Boston University (USA), and Graz University (Austria), respectively.

We selected 42 samples from Hole U1341B, which were freeze-dried and hand-powdered with an agate mortar and pestle. Digestion and instrumental analysis of the samples took place at KBSI. The samples were

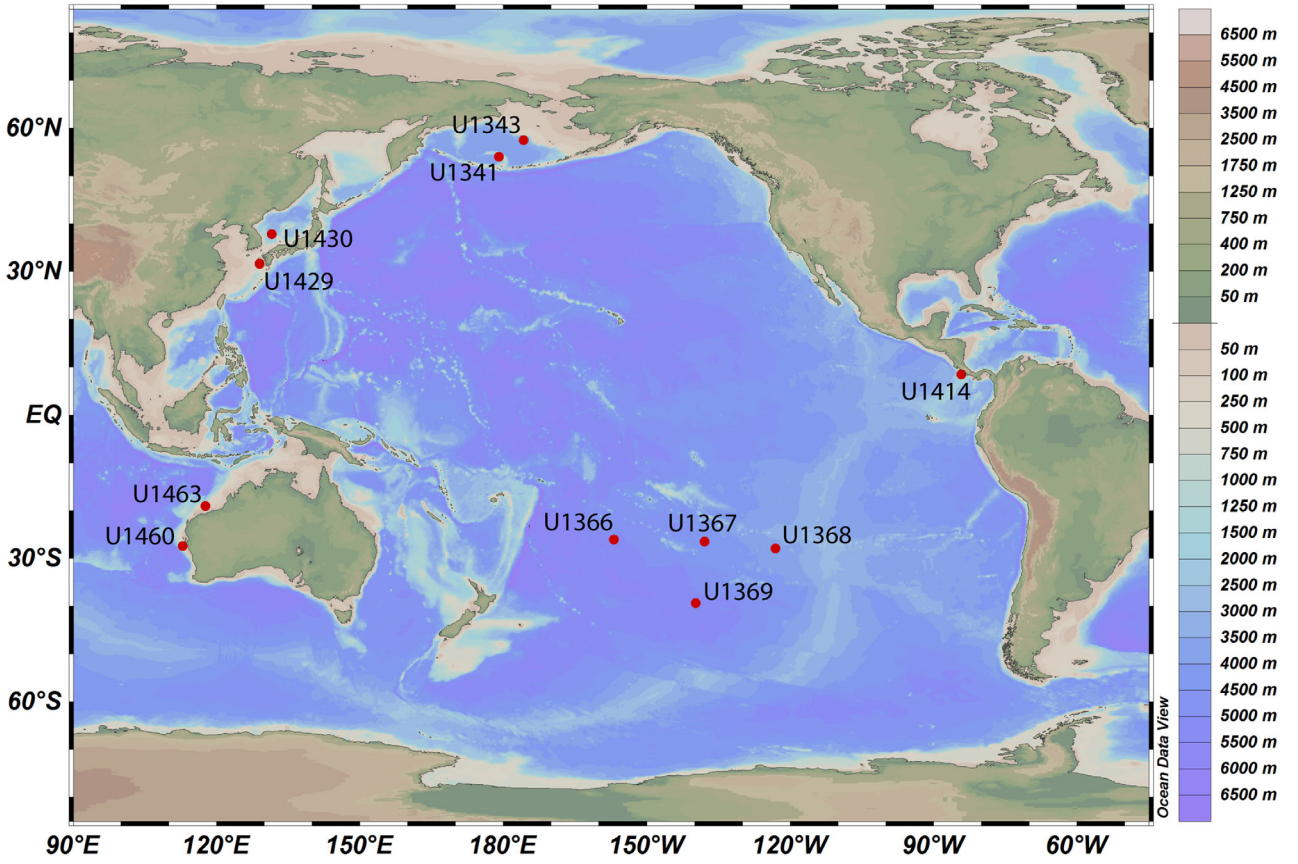

Figure 2. Map of IODP sites utilized in this study.

digested twice, first with a 4:4:1 mixture of HNO_3, HF, and $HClO_4$, then by $HClO_4$ and boric acid in a Teflon digestion vessel. Samples were redissolved in diluted HNO_3 and analyzed on a PerkinElmer OPTIMA 8300 ICP-ES for K content and on a Thermo X series ICP-MS for U and Th content. The long-term precision at KBSI is $<$5% for K and $<$10% for U and Th. The accuracy was determined through analysis of a standard BCR-2 (Basalt, Columbia River, USGS), for which the results were consistent with certified values [*Raczek et al*., 2001].

We selected 24 samples from Hole U1428A, 28 samples from Hole U1429A, and 50 samples from Hole U1430A. Samples were prepared and analyzed at Boston University and details of the analytical approach can be found in *Dunlea et al*. [2015]. In brief, we first freeze-dried and hand-powdered the samples with an agate mortar and pestle. For K content, sample powders were digested via a lithium metaborate flux fusion technique and the solutions were run on a Jobin Yvon Ultima C ICP-ES. For U and Th contents, sample powders were dissolved in a heated acid cocktail (HNO_3, HCl, and HF, with a later addition of H_2O_2), dried down, and then redissolved in HNO_3 and H_2O_2 under clean lab conditions. Solutions were diluted and analyzed on a VG PlasmaQuad Excell ICP-MS. Three separate digestions of an in-house standard run with each batch of samples determined the precision of the K, U, and Th contents to be 2%, 2.5%, and 2%, respectively, of the measured values. In each run, we analyzed a standard reference material (BHVO-2) as an unknown and contents were repeatedly accurate within precision.

The 15 samples from Hole U1463B were digested using the lithium metaborate flux fusion technique. We measured the solutions at Graz University (Austria) using an Agilent 7500 ICP-MS. We ran several international standards as unknowns (ML-2, JCp1, and JLS1) to check accuracy. Standards were accurately reproduced with a precision of $\sim$5% for K, U, and Th, based on the values provided in the GeoReM database [*Jochum et al*., 2005].

Given the agreement of standards run with their International Standard Reference Material (SRM) compositions, we consider the ICP data to accurately reflect the element content of K, U, and Th in the sediment, allowing for an evaluation of the NGR-based estimates.

2.2. Quantifying K Contents Using XRF

We expand the evaluation of the algorithm's performance by also considering K contents measured by quantitative wavelength-dispersive X-Ray fluorescence (XRF). We use 112 samples from Site U1341 and 41 samples from Site U1343 (Exp. 323) obtained by discrete plastic scoops (2 cm thickness). The XRF results from Site U1341 were previously published by *März et al*. [2013]. Sediment samples were freeze-dried, ground, mixed with 4200 mg di-lithiumtetraborate ($Li_2B_4O_7$, Spectromelt A10), preoxidized at 500°C with $\sim$1.0 g NH_4NO_3 (p.a.), fused to homogenous glass beads, and analyzed by wavelength-dispersive X-ray fluorescence (Panalytical PW 2400) at the Institute for Chemistry and Biology of the Marine Environment (ICBM) at Oldenburg University (Germany). Analytical precision and accuracy were better than 5% as checked by in-house and international SRMs. The precision of the XRF measurements of K content is only slightly less constrained than the precision of the ICP-ES measurements. Therefore, we add the XRF-based K contents to the ICP-ES data set to enlarge it for the evaluation of the algorithm.

3. Quantifying K, U, and Th Contents Using Shipboard Natural Gamma Radiation Spectra: Description of the Algorithm

The algorithm provided in this study consists of two MATLAB scripts. The first, *Extract_NGR_spectra.m*, extracts the NGR spectra from the .zip files available for download from IODP's LIMS Online Reports database. Subsequently, this script subtracts a measured zero-background and applies an edge-correction for those measurements taken within 20 cm from a core section's end cap (Figure 3). The second script, *Quantification_K_U_Th.m*, provides an estimate of the K, U, and Th contents by integrating NGR counts over specific energy intervals, and by comparing those counts to energy spectra of measured standards. The files *energylevels_K.mat, energylevels_Th.mat*, and *energylevels_U.mat* contain the NGR energy spectra of the standards and are thus required to run the algorithm.

3.1. Handling of .zip Files

The full NGR spectrograms can be downloaded from the LIMS Online Reports database (LORE; http://web.iodp.tamu.edu/LORE/). This database contains samples and data for IODP expeditions since March 2009

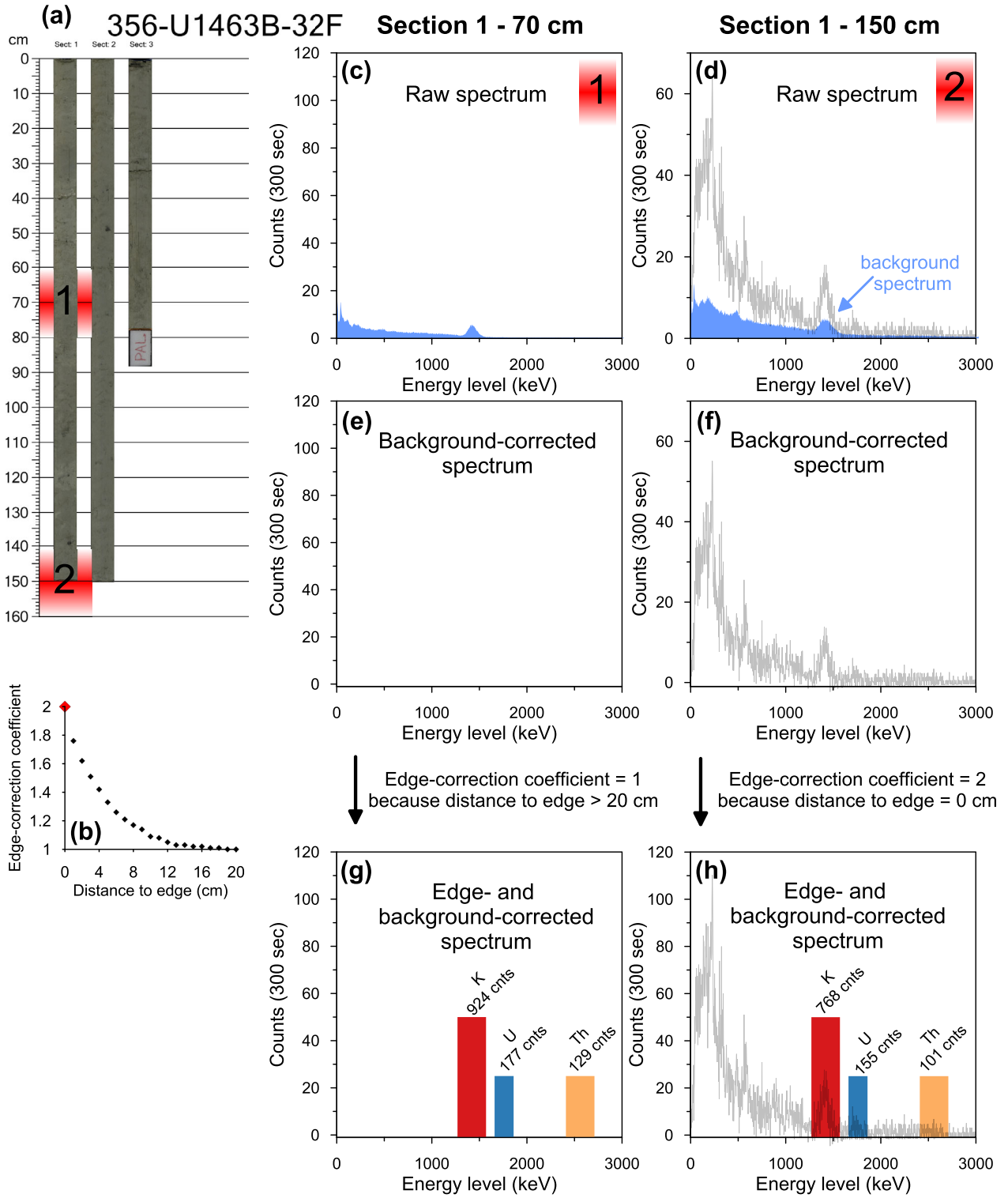

Figure 3. Schematic description of the algorithm. (a) Core Composite image of Core U1463B-31F, consisting of homogenous mudstone. The two depth intervals highlighted in red produced the NGR spectra used in Figures 3c–3h of this figure. (b) Edge-correction coefficient as a function of the distance between the detector and the edge of the measured core section. (c and d) Raw NGR spectra (black) with the background spectra (blue) produced by the sediment highlighted in Figure 3a of this figure. (e and f) The two NGR spectra after subtraction of the measured background spectrum. (g and h) Because the NGR spectrum from the second depth interval is taken closer than 20 cm from a section edge, the spectrum counts are multiplied by an edge-correction coefficient. Counts of the spectra from both depth intervals are then integrated over three energy intervals characteristic of K (red), U (blue), and Th (yellow). The integrated counts are subsequently compared to the corresponding peak in the spectra of a known standard (Figure 1) and adjusted for density to produce K, U, and Th concentrations for both of the depth intervals.

(Expedition 317 onward). The spectrograms are available for download as an *expanded report* under the *Natural Gamma Radiation (NGR)* tab. By clicking on the *batch download linked files* button, a Java application is downloaded, through which a file downloader can be opened. Then, select *archive_asman_id* as a report column and click *Download*. The requested NGR spectrograms will be downloaded as .zip files to the selected directory [Figure 9 in *Vasiliev et al*., 2011].

3.2. Subtraction of a Measured Zero-Background

A background spectrum is measured whenever the ship changes position, even if by only a few kilometers (Figure 3). In practice, however, short transit times and backlogs in NGR measurements often result in background spectra only measured after multiday transits. Background spectra are measured by loading an empty core liner in the titanium core "boat" that carries the section into the NGR instrument, to simulate conditions similar to the measurements of actual core sections. The measurement time, however, is much longer for background measurements (5–6 h) than for routine measurements (300 s) [*Vasiliev et al*., 2011]. The zero-background measurements are also contained in the above mentioned .zip files as 16 data files, each of which contains the zero-background spectrum of a specific detector at a specific measurement position [*Expedition 323 Scientists*, 2011; *Vasiliev et al*., 2011]. For each NGR sample measurement, the MATLAB algorithm seeks out which sodium iodide (NaI) detector has taken the measurement, and at which measurement position. Based on this information, the algorithm subtracts the corresponding zero-background measurement from the sample's NGR spectrogram (lines 125–138 in *Extract_NGR_spectra.m*, Figure 3).

3.3. Section Edge Correction

A NaI detector receives NGR from the core sample directly covering the detector, as well as from a "visible range" of ~20 cm on either side of the detector (i.e., the axial length of the detectors' response function: Figures 4 and 5 in *Vasiliev et al*. [2011]). When a detector's visible range is not fully covered by cored material, an edge correction needs to be applied (lines 140–171 in *Extract_NGR_spectra.m*, Figure 3). For every section, the blue end cap (section top) will directly cover the last NaI detector at measurement position 1. This implies that only half of the visible range of that detector will be covered by cored material, and therefore the measured NGR spectrum is multiplied by the edge effect correction coefficient (which is 2 in this case). The edge effect correction coefficient depends on the distance between a core section's edge and the center of the last detector directly covered by core sample. In the example above, this distance is 0 cm and the correction coefficient is 2. For distances between 0 and 20 cm, the correction factors were empirically determined at 1 cm intervals by *Vasiliev et al*. [2011; Figure 3].

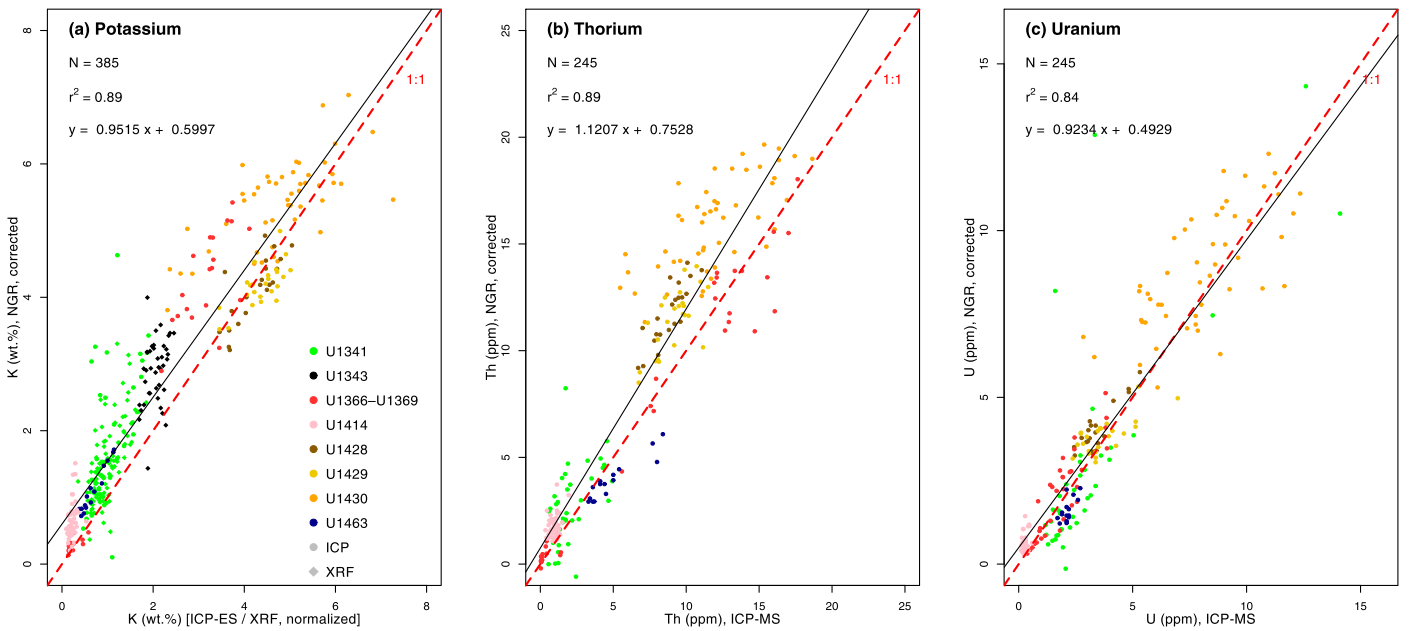

Figure 4. Total K, Th, and U contents measured by ICP-ES/MS or XRF compared to density-corrected K, Th, and U contents measured by NGR. Potassium contents measured by ICP-ES were normalized to anhydrous values.

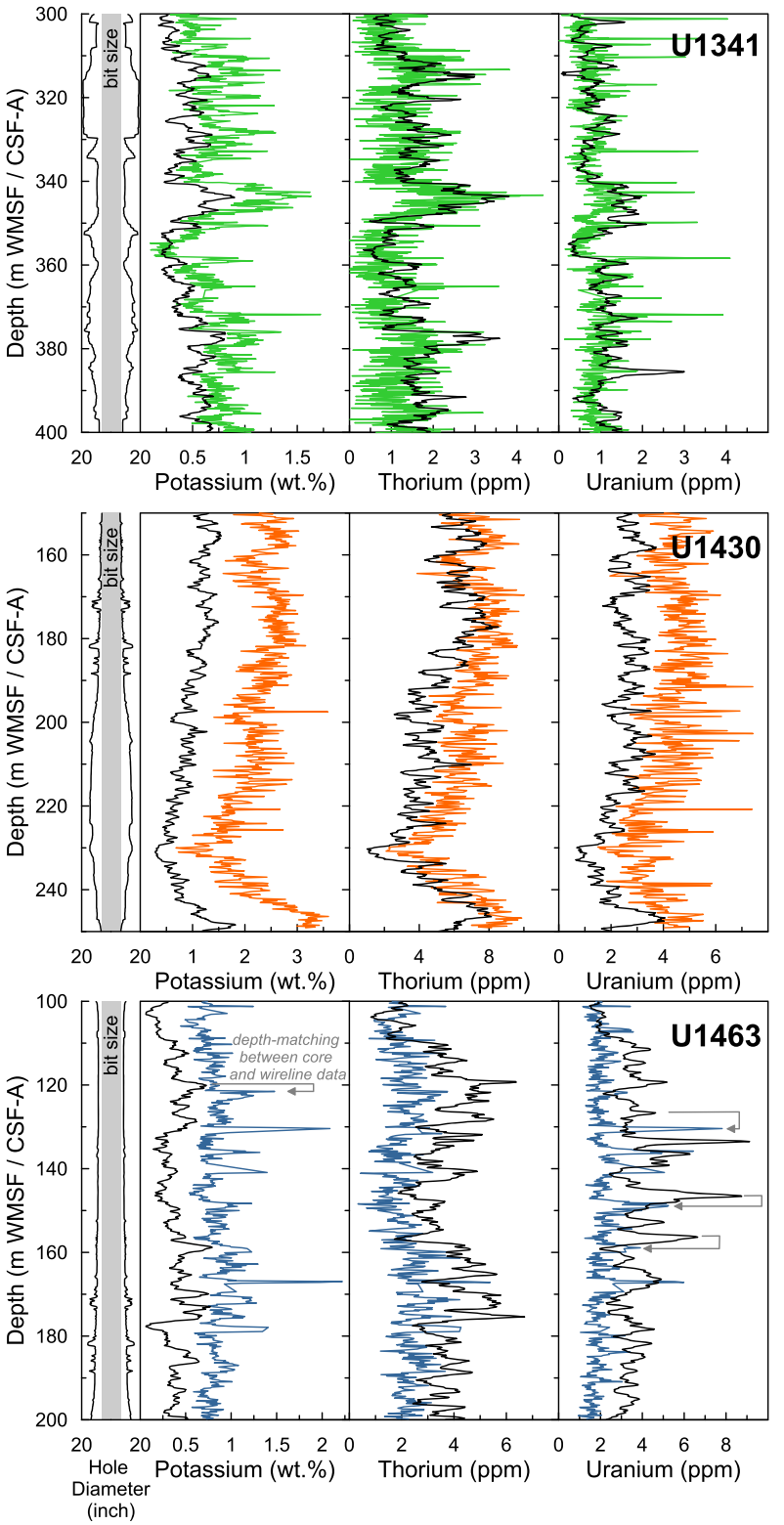

Figure 5. Comparison of core-based NGR-derived element contents (green: U1341; orange: U1430; blue: U1463) with downhole wireline logging results (black). Borehole diameter is measured by the triple combination toolstring's caliper. The wireline element contents are based on NGR measurements taken by the Hostile Environment Natural Gamma Ray Sonde (HNGS) and were corrected for hole size during the recording. Core-based NGR-derived contents are plotted along the CSF-A depth scale; downhole logging results are shown along the WMSF depth scale [*IODP*, 2011]. Both depth scales are not necessarily the same, as demonstrated by the grey arrows at Site U1463. The grey arrows indicate possible tie-points for depth-matching between both depth scales.

3.4. The Quantification of K, U, and Th Contents

In this study, the estimates of K, U, and Th contents are based on a calibration carried out by measuring one shipboard standard per element on all detectors. These single-nuclide standard sources, produced by Isotope Products Laboratories (Burbank, California), contain their respective K, U and Th content homogenously distributed in an epoxy (K and Th) or plaster (U) matrix, filling a ~50 cm long cylinder with the same diameter as a core liner. The standards' contents were converted from the amount of radioactivity reported for the standards ($K_{standard}=6.43\ wt.\%$, $U_{standard}=0.187\ ppm$, $Th_{standard}=20.7\ ppm$). The standards' densities were measured on the shipboard Gamma Ray Attenuation (GRA) system, installed on the whole-round multisensor logger (WRMSL), during IODP Exp. 356 ($\rho_{K\_standard}=2.07\ \frac{g}{cm^3}$, $\rho_{U\_standard}=2.23\ \frac{g}{cm^3}$, $\rho_{Th\_standard}=2.16\ \frac{g}{cm^3}$). Given a NGR spectrum of a sample of unknown composition, these calibration measurements convert the detected gamma rays at specific energy ranges into element content estimates. In our algorithm, the first step is integration of the ^{40}K, ^{214}Bi, and ^{208}Tl peak in the background-subtracted and edge-corrected spectrum of all samples (lines 44, 132, and 194 in *Quantification_K_U_Th.m*, Figure 3). The energy ranges over which these characteristic peaks in the NGR spectrum are integrated are shown in Figures 1 and 3g and 3h. The algorithm divides the area under the spectral peak in question (A_{sample}) by the equivalent area in the spectrum of the standard ($A_{standard}$) (lines 50, 138 and 200 in *Quantification_K_U_Th.m*). The counts in the U and Th windows are less than the counts in the K window (Figures 3g and 3h), which can introduce noise in the U and Th spectra and resulting concentration data. To incorporate the probability of a decay event being observed in their low-count spectra, *Dunlea et al*. [2013] adopted a slightly different method and compared the measured NGR spectra to spectra generated by Monte Carlo simulations to obtain U and Th concentrations. Here we show that counts in the U and Th windows are sufficient (Figures 3g and 3h) to accurately estimate the U and Th element content in the sample after a 5 min measurement (Figures 4b and 4c). Additional U and Th standards for the NGR instrument with higher concentrations of U and Th would improve the conversion of counts to concentrations.

Subsequently, we take into account the density difference between sample and standard. The sample's bulk density is an essential sediment property in the quantification of K, U, and Th contents because for two samples with equal element contents but different densities, the detectors will receive more NGR while measuring the denser sample (assuming the sample volume is identical, which is usually the case with a sediment-filled core liner). The bulk density of the sediment volume from which the detector receives NGR ($\rho_{bulk,ample}$) is calculated by applying a Gaussian smoothing of all GRA measurements within a range of 20 cm on either side of the detector (line 72 in *Quantification_K_U_Th.m*). The Gaussian weight function represents the NGR detector response function [Figures 4 and 5 in *Vasiliev et al*., 2011; integration length of ~40 cm]. This procedure is analogous to the strategy developed by *Walczak et al*. [2015], who utilized GRA bulk density to generate mass-specific NGR total counts. Bulk density is commonly measured at 5 cm intervals by the GRA system and can be downloaded from the LORE database. Be sure to select the WRMSL instrument option. Finally, the NGR-based estimates of K, U and Th contents are calculated using equations (1–3), respectively.

$$K(wt.\%)_{NGR}=\frac{A_{sample}}{A_{standard}}\cdot\frac{\rho_{K\_standard}}{\rho_{bulk\_sample}}\cdot K(wt.\%)_{standard} \quad (1)$$

$$U(ppm)_{NGR}=\frac{A_{sample}}{A_{standard}}\cdot\frac{\rho_{U\_standard}}{\rho_{bulk\_sample}}\cdot U(ppm)_{standard} \quad (2)$$

$$Th(ppm)_{NGR}=\frac{A_{sample}}{A_{standard}}\cdot\frac{\rho_{Th\_standard}}{\rho_{bulk\_sample}}\cdot Th(ppm)_{standard} \quad (3)$$

4. Discussion

4.1. Comparing NGR-Derived With ICP-ES, ICP-MS, and XRF-Derived Element Contents

Our algorithm uses GRA bulk density to estimate several of its chemical constituents. This bulk density represents a *wet* density and is thus a function of grain density and porosity. In contrast, the ICP-ES, ICP-MS, and XRF analyses were carried out on freeze-dried samples. This implies that the measured element contents are based on a *dry* sample weight. Similar to *Dunlea et al*. [2013], we found a density correction was required prior to the comparison of NGR-derived estimates with ICP and XRF measurements (equations (4–6)).

The density correction factor consists of the ratio between *wet* bulk density and *dry* grain density [*Dunlea et al*., 2013]. We use shipboard moisture and density (MAD) data to determine this ratio, and to correct the NGR-based estimates for direct comparison with the ICP and XRF-based measurements.

$$K(wt.\%)_{NGR,corrected} = \frac{\rho_{bulk}}{\rho_{dry}} K(wt.\%)_{NGR} \quad (4)$$

$$U(ppm)_{NGR,corrected} = \frac{\rho_{bulk}}{\rho_{dry}} U(ppm)_{NGR} \quad (5)$$

$$Th(ppm)_{NGR,corrected} = \frac{\rho_{bulk}}{\rho_{dry}} Th(ppm)_{NGR} \quad (6)$$

As noted by *Dunlea et al*. [2013], shipboard MAD bulk and dry densities are determined after drying the sample in a convection oven at 105°C for 24 h, potentially removing interlayer water from clay minerals and CO_2 from carbonates. Freeze-drying the sediment, on the other hand, retains the interlayer water and CO_2. This implies that baking versus freeze-drying sediment can result in noticeable differences in dry weight. To account for this difference, *Dunlea et al*. [2013] normalized the major oxides (including K_2O) to sum to 100%. In this study, we follow their procedure and calculate "volatile-free" ICP-ES data to generate the most appropriate K contents to compare to the density-corrected NGR data.

We evaluate the accuracy and precision by which the MATLAB algorithm quantifies K, U, and Th contents using a series of cross-plots (Figure 4). These cross-plots show density-corrected NGR-derived K contents as a function of normalized ("volatile-free") ICP-ES or XRF data, and density-corrected NGR-derived U and Th contents as a function of their corresponding ICP-MS measurement. The precision of the algorithm is evaluated by the correlation coefficient and the accuracy by the slope and intercept of a linear model fitted to the data. An algorithm that produces accurate chemical data estimates will result in a regression line with a slope close to 1 and an intercept close to 0.

The correlation between the different K measurements is strong ($R^2 = 0.89$), but a few outliers degrade the correlation (Figure 4a). Nevertheless, these outliers have only a minor influence on the slope (0.95) and intercept (0.60). These are close to the expected values, and thus suggest that the algorithm makes accurate estimates of the sediment's K content.

The correlation coefficient for Th is equally high ($R^2 = 0.89$, Figure 4b). In the cross plot for Th, no obvious outliers can be observed and the precision of the algorithm clearly degrades with higher Th contents. The slope (1.12) and intercept (0.75) of the linear regression suggest that the algorithm is slightly overestimating Th contents.

The correlation coefficient for U is almost as good as that for K and Th ($R^2 = 0.84$, Figure 4c). The slightly lower correlation may be the result of a few outliers from Site U1341 and scatter in the data from Site U1430, where relatively high U content is observed. The linear regression line straddles the 1:1-line (slope = 0.92, intercept = 0.49), indicating that the algorithm produces highly accurate estimates of the sediment's U content.

The overall conclusion is that the algorithm produces accurate estimates of K, U, and Th contents with acceptable precision (Figure 4). Some of the main reasons for the limited precision have to do with the different density measurements (GRA and MAD). One source of scatter is when cores have fractures and gaps in the sediment and emit less NGR simply because less sediment is present. Much of this effect is accounted for by the GRA bulk density correction described above. However, when fractures or gaps in the sediment coincidentally match GRA measuring positions every ~5 cm, the GRA bulk density measurements can underestimate the true *wet* bulk density of the sediment seen by the NGR detector, and thus result in an overestimation of NGR-derived K, U, and Th contents. A second potential issue with the GRA bulk density data is that one assumes the Compton gamma-ray attenuation coefficient is the same for different lithologies. Violations of this assumption can result in errors in GRA bulk density measurements of up to 5% [*Blum*, 1997]. A third reason for the scatter in Figure 4 comes from the fact that there is no colocated MAD measurement for every NGR measurement, thus requiring interpolation between different MAD data points. A fourth source of error originates from the difference in spatial resolution between the NGR-derived and ICP or XRF-derived element contents. The NGR system integrates counts from a 40 cm long portion of the core,

whereas most of the ICP and XRF measurements were carried out on samples gathered from 2 cm thick intervals. Finally, a fifth source of error for U contents may occur in sediment younger than 1.5 Ma where the U-series decay chain is in secular disequilibrium [*Dunlea et al*., 2013]. U dissolved in the water column will decay to ^{230}Th, which is insoluble and removed to the seafloor. The subsequent decay products of ^{230}Th in the sediment include ^{214}Bi. The activity of ^{214}Bi is measured by the NGR instrument and used to infer U contents. Thus, the "excess" ^{230}Th from the water column that increases ^{214}Bi activity in the sediment can cause U contents derived from NGR spectra to appear higher than the actual U content in the sediment.

4.2. Comparing Core-Based NGR-Derived Element Contents With Downhole Wireline Logging Results

During many IODP expeditions, downhole wireline logging operations are executed in one or more boreholes. In those cases, the NGR of the formations is measured with the Hostile Environment Natural Gamma Ray Sonde [HNGS; *IODP-USIO*, 2003]. The HNGS discerns 256 energy levels, compared to the 1024 energy levels differentiated by the NGR system in the laboratory on DV *JOIDES Resolution*. The HNGS uses the same principles as the algorithm presented in this study to provide estimates of K, U, and Th contents, although the signal processing is proprietary. The ranges of the energy windows used to determine the content of each component are slightly different between the HNGS and this study (Figure 1). A second difference is the explicit consideration of formation bulk density in the presented core-based algorithm, whereas variations in formation bulk density can cause changes in the radius of investigation during wireline logging (with lower radioactivity in denser formations) [*IODP-USIO*, 2003]. Third, the wireline log-based content estimates depend on a correction for borehole size and potassium (KCl) in the mud used prior to logging to stabilize clays and avoid the formation of bridges [*IODP-USIO*, 2003]. Finally, the wireline NGR measurement time is only 1 s, which translates to a spatial resolution of ~15 cm, given a typical logging speed of about 550 m/h. As a result, wireline NGR measurements are characterized by large variability. This variability is reduced by considering NGR counts in the low-energy part of the spectrum (W1 and W2 in Figure 1) and by smoothing the data over three adjacent measurements [*IODP-USIO*, 2003]. Because of these differences and the good fit between core-based NGR-derived element contents and ICP/XRF measurements (Figure 4), we consider the core-based element contents more reliable than the downhole wireline logging results.

In Figure 5, we compare core-based NGR-derived element contents from Sites U1341, U1430, and U1463 with those obtained during downhole logging. Core-based K content estimates are consistently higher than wireline-derived contents, although the offset differs between the three sites. There seems to be no correlation between underestimation and hole diameter, which is to be expected since the downhole HNGS data for the three holes were corrected for hole size during the recording. The formation bulk density and porosity are similar at the three different sites, and thus cannot account for the different offsets between core-based and wireline estimates. Through elimination, we assume that the different offsets between sites are related to the mud correction of the downhole logging spectra. Despite the offset in absolute values, the core-based and wireline K content depth-series exhibit the same relative variations, allowing for depth-matching between core and wireline data (e.g., U1463 in Figure 5). This is an important issue (especially for sites without a stratigraphic splice) because cored depth-scales (e.g., CSF-A) are built incrementally with many potential sources of uncertainty, whereas the wireline matched depth-scale (WMSF) is continuously constructed based on the vertical speed of the logging tool [*IODP*, 2011].

Core-based Th and U contents are higher than wireline-derived contents at Site U1430, lower than wireline-derived contents at Site U1463, and similar to wireline-derived contents at Site U1341 (Figure 5). There is again no obvious reason for these differences in offset. However, the heavy drilling mud might also play a role here, as the density of the mud at the time of measurement influences the radius of investigation of the HNGS.

5. Conclusions

The International Ocean Discovery Program (IODP) and its predecessors play a crucial role in our understanding of ocean-climate systems. Here, we present a MATLAB algorithm that rapidly processes shipboard NGR data, allowing for the evaluation of the K, U, and Th contents of the cored material (and the ratios between these elements), which can contribute to future IODP-related discoveries. Importantly, these shipboard data can be processed in minutes and without any additional cost. Hence, this algorithm could be

useful for decision-making during expeditions, as well as produce insightful data for post cruise research. The algorithm quantifies K, U, and Th element contents by integrating energy spectra obtained during routine NGR measurements on-board the *JOIDES Resolution*. The key feature of the algorithm is the integration of NGR counts over element-specific energy intervals of the spectrum. A comparison of the algorithm's results with ICP-ES, ICP-MS, and XRF measurements of the element contents of K, U, and Th demonstrates that the algorithm provides accurate estimates, with satisfactory precision. The MATLAB scripts are freely available, relatively uncomplicated to use, and can be used to generate K, U, and Th elemental contents for all holes cored by *JOIDES Resolution* since Expedition 317.

Acknowledgments

We thank the IODP Expedition 323, 346, and 356 Shipboard science parties, the crew, and technical staff of DV *JOIDES Resolution* for help. We also thank C. Hauzenberger and W. Gössler for help with ICP-MS measurements. This project used samples and data provided by the International Ocean Discovery Program (IODP) and its predecessors. DDV is a postdoctoral researcher and HP is the principal investigator in ERC Consolidator grant "EarthSequencing" (grant agreement 617462). Portions of this material are based on work supported while RWM was serving at the National Science Foundation. All new data reported in this study can be obtained from PANGAEA (https://doi.pangaea.de/10.1594/PANGAEA.872654). We ran the algorithm for all holes cored JOIDES Resolution since Expedition 317: These datasets can be downloaded from http://daviddevleeschouwer.webs.com/ngr.htm.

References

Adams, J. A., and C. E. Weaver (1958), Thorium-to-uranium ratios as indicators of sedimentary processes: Example of concept of geochemical facies, *AAPG Bull.*, *42*(2), 387–30.

Blum, P. (1997), Physical properties handbook: A guide to the shipboard measurement of physical properties of deep-sea cores, *ODP Tech. Note 26*, Ocean Drill. Program, College Station, Tex.

Blum, P., A. Rabaute, P. Gaudon, and J. F. Allan (1997), Analysis of natural gamma-ray spectra obtained from sediment cores with the shipboard scintillation detector of the Ocean Drilling Program: Example from Leg 1561, in *Proceedings of the Ocean Drilling Program, Scientific Results*, edited by T. H. Shipley et al., pp. 183–195, Ocean Drill. Program, College Station, Tex.

Bond, D., and M. Zaton (2003), Gamma-ray spectrometry across the Upper Devonian basin succession at Kowala in the Holy Cross Mountains (Poland), *Acta Geol. Pol*, *53*(2), 93–99.

Brumsack, H.-J. (2006), The trace metal content of recent organic carbon-rich sediments: Implications for Cretaceous black shale formation, *Palaeogeogr. Palaeoclimatol. Palaeoecol.*, *232*(2–4), 344–361.

D'Hondt, S., et al. (2009), Subseafloor sedimentary life in the South Pacific Gyre, *Proc. Natl. Acad. Sci.*, *106*(28), 11,651–11,656.

De Vleeschouwer, D., M. Rakociński, G. Racki, D. P. Bond, K. Sobień, and P. Claeys (2013), The astronomical rhythm of Late-Devonian climate change (Kowala section, Holy Cross Mountains, Poland), *Earth Planet. Sci. Lett.*, *365*, 25–37.

Doveton, J. (1991), Lithofacies and geochemical facies profiles from nuclear wireline logs: New subsurface templates for sedimentary modelling, in *Sedimentary Modelling-Computer Simulations and Methods for Improved Parameter Definition*, edited by E. K. Franseen et al., pp. 101–110, Kansas Geol. Soc. Bull., Lawrence, Kansas.

Dunlea, A. G., R. W. Murray, R. N. Harris, M. A. Vasiliev, H. Evans, A. J. Spivack, and S. D'Hondt (2013), Assessment and use of NGR instrumentation on the JOIDES Resolution to quantify U, Th, and K concentrations in marine sediment, *Sci. Drill.*, *15*, 57–63.

Dunlea, A. G., R. W. Murray, J. Sauvage, A. J. Spivack, R. N. Harris, and S. D'Hondt (2015), Dust, volcanic ash, and the evolution of the South Pacific Gyre through the Cenozoic, *Paleoceanography*, *30*, 1078–1099, doi:10.1002/2015PA002829.

Expedition 323 Scientists (2011), Methods, in *Proceedings of the Integrated Ocean Drilling Program*, edited by K. Takahashi et al., Tokyo.

Gallagher, S. J., C. S. Fulthorpe, and K. A. Bogus (2014), *Reefs, Oceans, and Climate: A 5 Million Year History of the Indonesian Throughflow, Australian Monsoon, and Subsidence on the Northwest Shelf of Australia*, Int. Ocean Discovery Program, College Station, Tex.

Gilmore, G. (2011), *Practical Gamma-Ray Spectroscopy*, John Wiley, Warrington, U. K.

Hassan, M., and A. Hossin (1975), Contribution à l'étude des comportements du thorium et du potassium dans les roches sédimentaires, *C. R. Acad. Sci. Paris*, *280*, 533–535.

Hassan, M., A. Hossin, and A. Combaz (1976), Fundamentals of the differential gamma ray log-interpretation technique, paper presented at SPWLA 17th Annual Logging Symposium, Soc. of Petrophys. and Well-Log Anal., Denver, Colo.

Humphreys, B., and G. K. Lott (1990), An investigation into nuclear log responses of North Sea Jurassic sandstones using mineralogical analysis, in *Geological Application of Wireline Logs*, edited by A. Hurst, M. A. Lovell and A. C. Morton, Geol. Soc. Spec. Publ., 48, 223–240.

Hurst, A. (1990), Natural gamma-ray spectrometry in hydrocarbon-bearing sandstones from the Norwegian Continental Shelf, in *Geological Application of Wireline Logs*, edited by A. Hurst, M. A. Lovell, and A. C. Morton, Geol. Soc. Spec. Publ., 48, 211–222.

International Atomic Energy Agency (1976), Radiometric reporting methods and calibration in uranium exploration, *Tech. Rep. Ser.*, *174*, pp. 57, Vienna, Austria.

IODP (2011), *IODP Depth Scales Terminology*, College Station, Tex. [Available at http://www.iodp.org/policies-and-guidelines/142-iodp-depth-scales-terminology-april-2011/file, accessed 26 Oct. 2016.]

IODP-USIO (2003), Downhole Logging *Tools*, College Station, Tex. [Available at http://iodp.ldeo.columbia.edu/TOOLS_LABS/MULT/hngs.html, accessed 26 Oct. 2016.]

Jochum, K. P., U. Nohl, K. Herwig, E. Lammel, B. Stoll, and A. W. Hofmann (2005), GeoReM: A new geochemical database for reference materials and isotopic standards, *Geostand. Geoanal. Res.*, *29*(3), 333–338.

März, C., B. Schnetger, and H. J. Brumsack (2013), Nutrient leakage from the North Pacific to the Bering Sea (IODP Site U1341) following the onset of Northern Hemispheric Glaciation?, *Paleoceanography*, *28*, 68–78, doi:10.1002/palo.20011.

Myers, K. J., and P. B. Wignall (1987), Understanding Jurassic Organic-rich Mudrocks—New Concepts using Gamma-ray Spectrometry and Palaeoecology: Examples from the Kimmeridge Clay of Dorset and the Jet Rock of Yorkshire, in *Marine Clastic Sedimentology: Concepts and Case Studies*, edited by J. K. Leggett and G. G. Zuffa, pp. 172–189, Springer, Dordrecht, Netherlands.

Myers, K. J., and C. S. Bristow (1989), Detailed sedimentology and gamma-ray log characteristics of a Namurian deltaic succession II: Gamma-ray logging, *Geol. Soc. Spec. Publ.*, *41*(1), 81–88.

Raczek, I., B. Stoll, A. W. Hofmann, and K. P. Jochum (2001), High-Precision Trace Element Data for the USGS Reference Materials BCR-1, BCR-2, BHVO-1, BHVO-2, AGV-1, AGV-2, DTS-1, DTS-2, GSP-1 and GSP-2 by ID-TIMS and MIC-SSMS, *Geostand. Newsl.*, *25*(1), 77–86.

Serra, O. (1984), 7. Natural Gamma-Ray Spectrometry, in *Developments in Petroleum Science*, edited by O. Serra, pp. 113–134, Elsevier, Amsterdam, The Netherlands.

Tada, R., R. W. Murray, C. Alvarez Zarikian, and the Expedition 346 Scientists (2015), *Proceedings of IODP*, Integrated Ocean Drill. Program, College Station, Tex.

Takahashi, K., A. C. Ravelo, C. Alvarez Zarikian, and the IODP Expedition 323 Scientists (2011), IODP Expedition 323: Pliocene and Pleistocene Paleoceanographic Changes in the Bering Sea, Sci. Dril., *11*, 4–13.

Vasiliev, M., P. Blum, G. Chubarian, R. Olsen, C. Bennight, T. Cobine, D. Fackler, M. Hastedt, D. Houpt, and Z. Mateo (2011), A new natural gamma radiation measurement system for marine sediment and rock analysis, *J. Appl. Geophys.*, *75*(3), 455–463.

Walczak, M. H., A. C. Mix, T. Willse, A. Slagle, J. S. Stoner, J. Jaeger, S. Gulick, L. LeVay, A. Kioka, and the IODP Expedition 341 Scientific Party (2015), Correction of non-intrusive drill core physical properties data for variability in recovered sediment volume, *Geophys. J. Int.*, *202*(2), 1317–1323.

Wignall, P. B., and R. J. Twitchett (1996), Oceanic anoxia and the end permian mass extinction, *Science*, *272*(5265), 1155–1158.

Yan, Q., and X. Shi (2016), Data report: Major and trace element and Sr-Nd-Pb isotope analyses for basement rocks from the CRISP-A transect drilled during Expeditions 334 and 344., in *Proceedings of the Integrated Ocean Drilling Program*, edited by R. N. Harris et al., Integrated Ocean Drill. Program, College Station, Tex.

Erratum

In the originally published version of this article, Software S1 and S2 files were inadvertently omitted from the Supporting Information. These files have since been added and this version may be considered the authoritative version of record.